Proceedings of Meetings on Acoustics

Volume 9, 2010 http://asa.aip.org

159th Meeting
Acoustical Society of America/NOISE-CON 2010
Baltimore, Maryland
19 - 23 April 2010
Session 2pBB: Biomedical Ultrasound/Bioresponse to Vibration

2pBB2. Analytic and numerical modeling of ultrasonic B-scan and echo decorrelation imaging

T. D. Mast* and Swetha Subramanian

***Corresponding author's address: Biomedical Engineering, University of Cincinnati, Cincinnati, OH 45267-0586, doug.mast@uc.edu**

An numerical model is presented for B-scan images of weakly-scattering,lossy media, based on ultrasound array beam patterns calculated analytically under the Fresnel approximation. Given these beam patterns and a 3D analytic or numerical tissue model, this method yields beamformed A-line signals from which B-scan images are constructed. This approach is further employed to model echo decorrelation imaging, a method for quantitatively mapping transient heat-induced changes in pulse-echo ultrasound images. In echo decorrelation imaging, a normalized decorrelation parameter is computed between A-line signals separated by milliseconds. Maps of this parameter comprise echo decorrelation images, which are potentially useful for monitoring of local tissue coagulation during thermal ablation treatments for cancer therapy. Following previous studies in which scattering cross section has been related to spatial-frequency spectra of tissue sound speed, density, and impedance variations, echo decorrelation is related quantitatively to the local decoherence of these spatial-frequency spectra. Decoherence estimates are validated by simulations employing analytic array beam patterns and random-media models for ablated tissue, and are further applied to quantify tissue structure changes caused by thermal coagulation during in-vitro radiofrequency ablation.

Published by the Acoustical Society of America through the American Institute of Physics

 [DOI: 10.1121/1.3483555]
Received 1 Jul 2010; published 6 Aug 2010

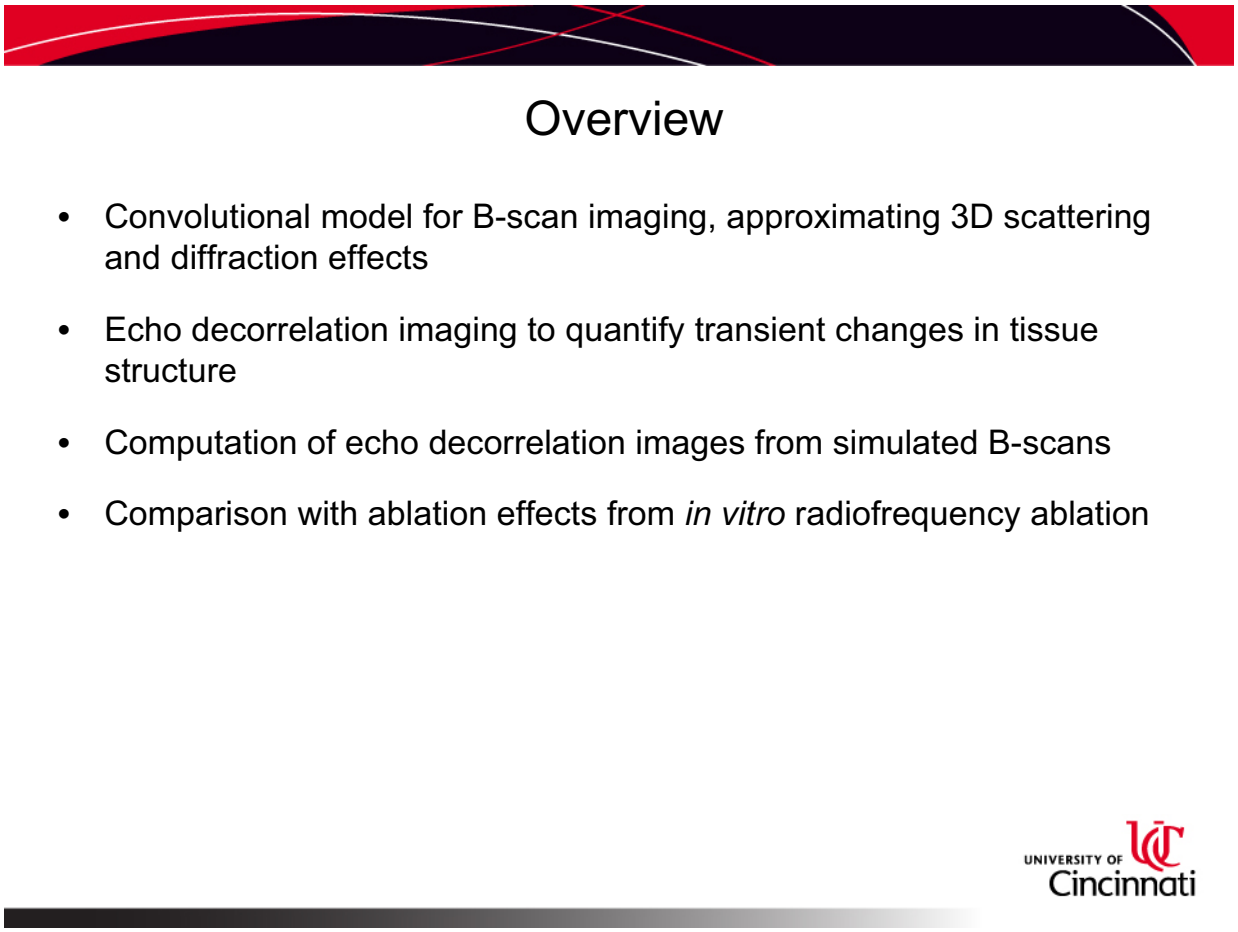

The slides included here comprise an entire invited presentation given at the 159th meeting of the Acoustical Society of America. The presentation reviews a convolution-based approach to analysis and simulation of B-scan ultrasound imaging (Mast 2010). This model is then employed to simulate and analyze echo decorrelation imaging (Mast 2008), an approach to real-time ultrasound monitoring of thermal ablation for cancer treatment.

B-scan imaging

- Linear array performs pulse-echo imaging of a 3D, linear, weakly scattering, lossy medium

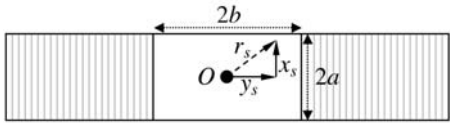

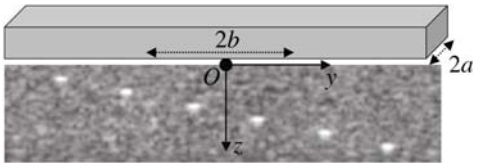

- Array transmits focused pulses along multiple lines

$$p_s(\mathbf{r}_s,t) = \frac{k^2\, e^{-i\omega t}}{4\pi} \int_{V_0} a\left(t - \frac{|\mathbf{r}_0 - \mathbf{r}_s| - r_0}{c}\right) \gamma(\mathbf{r}_0)\, p_E(\mathbf{r}_0)\, \frac{e^{ik|\mathbf{r}_0 - \mathbf{r}_s|}}{|\mathbf{r}_0 - \mathbf{r}_s|}\, dV_0$$

- System synthetically focuses scattered signals at multiple depths
- A-lines: beamformed echo signals for each line
- B-scan: echo brightness vs. position in medium

UNIVERSITY OF Cincinnati

The present model for pulse-echo ultrasound imaging applies to scattering media similar to soft tissues, which can be modeled as weakly scattering (Waag 1993). When a transient incident wave is transmitted from a portion of an ultrasound array, the resulting scattered field $p_s(\mathbf{r}, t)$ is approximated by the above equation (Morse 1968; Jansson 1998), in which ω is the center radial frequency of the transmitted pulse $a(t)\, e^{-i\omega t}$, k is the corresponding acoustic wave number, γ is the medium's position-dependent reflectivity, and p_E is the single-frequency beam pattern of the transmit aperture at the radial frequency ω. The integral is performed over the entire scattering volume V_0.

For B-scan (brightness mode) imaging, an ultrasound array transmits short, focused pulses into the medium. The scattered field is then received by a number of array elements and the resulting signals are synthetically focused by delay-and-sum operations. The resulting position-dependent signal amplitude is displayed as the local B-scan image brightness.

B-scan image model

- B-scan model: scattered signals integrated over effective (depth-dependent focus) detector surface
- A-lines $u(t)$ depend on medium reflectivity γ, pulse envelope a, emitter/detector beams p_E, p_D:

$$u(t) = \frac{ik\, e^{-i\omega t}}{2\rho c v_0} \int_{V_0} a\left(t - \frac{2z_0}{c}\right) \gamma(\mathbf{r}_0)\, p_E(\mathbf{r}_0)\, p_D(\mathbf{r}_0)\, dV_0,$$

- Diffraction effects summarized by "system function" Λ:

$$\Lambda(x_0, y_0, z_0) = p_E(\mathbf{r}_0)\, p_D(\mathbf{r}_0)$$

- Complex B-scan image $I(y,z)$ written in convolutional form:

$$I(y,z) = \left[u\left(\frac{2z}{c}\right)\right]_{(0,y,0)} = \frac{ik\, e^{-i\omega t}}{2\rho c v_0}\, a\left(\frac{2z}{c}\right) \otimes_z \int_x \gamma(\mathbf{r}) \otimes_y \Lambda(\mathbf{r})\, dx$$

UNIVERSITY OF Cincinnati

To model this image-formation process, the scattered field $p_s(\mathbf{r}, t)$ is integrated over effective (position-dependent) receiving apertures with size and focal characteristics equivalent to the receiving array subapertures of the imaging system simulated, including depth-dependent electronic focusing. The result of this model is an analytic expression for a complex A-line signal $u(t)$, in which $\rho c v_0$ is the nominal surface pressure amplitude and p_D is the single-frequency beam pattern of the effective receiving aperture.

Transmit and receive aperture effects can be compactly represented by a "system function" Λ (Waag 1993; Jansson 1998), defined here as a product of the single-frequency, complex transmit and receive beams. A complex B-scan image $I(y, z)$ is then expressed by the third equation above as a series of one-dimensional convolution and integration operations performed on the 3D medium reflectivity, the 3D system function, and the temporal transmit pulse envelope.

Model-experiment comparison

- Scattering medium mimicking ATS 539 ultrasound phantom
- Parameters matching 7 MHz, 192-element linear array system with dynamic receive focusing
- System function Λ computed by Fresnel approximation for focused, depth-dependent, rectangularly symmetric apertures
- Model includes frequency-dependent attenuation, sound speed mismatch, electronic noise, time-gain compensation

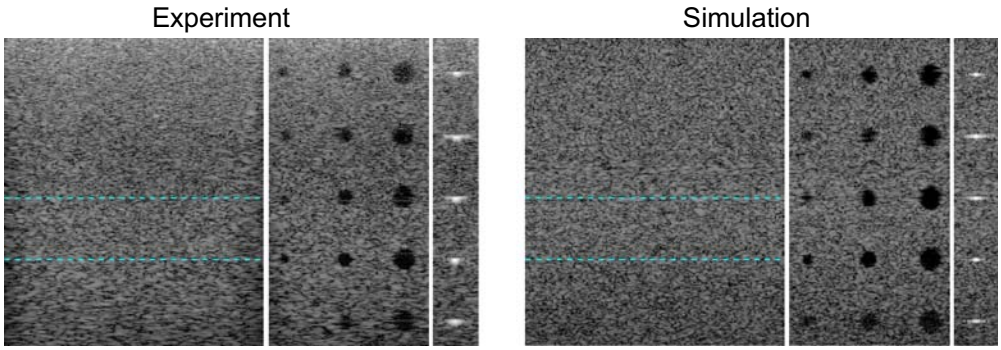

UNIVERSITY OF Cincinnati

Here, 7 MHz B-scan images of a standard ultrasound quality-assurance phantom (Model 539, ATS Laboratories) is simulated and compared with corresponding measured B-scans for the modeled transducer and imaging system (L7 and Iris 2, Ardent Sound). The scattering medium was modeled by defining a reflectivity function on a 3D grid. Transmit and receive beams were computed using a Fresnel approximation for focused rectangular apertures with error-function apodization (Mast 2007). Finally, the above equation for the complex B-scan image $I(y, z)$ was solved numerically (MATLAB, The Mathworks), with one-dimensional convolutions computed by fast Fourier transforms and integration performed by discrete summation. Before display, synthetic electronic noise was added and exponentially depth-dependent gain was applied to compensate for attenuation in the scattering medium.

The simulated image, which displays $|I(y, z)|$ on a logarithmic gray scale with 60 dB dynamic range, is comparable to the measured B-scan in depth-dependent speckle texture, resolution, and contrast. Successfully simulated effects include focus aberration caused by the discrepancy between the system-assumed sound speed (1.54 mm/μs) and the sound speed of the polyurethane phantom material (1.45 mm/μs). The main feature not accurately simulated is asymmetry of the wire targets in the depth direction.

Speckle statistics

- Speckle amplitude follows Rayleigh distribution
- Azimuthal autocorrelation function agrees with experiment

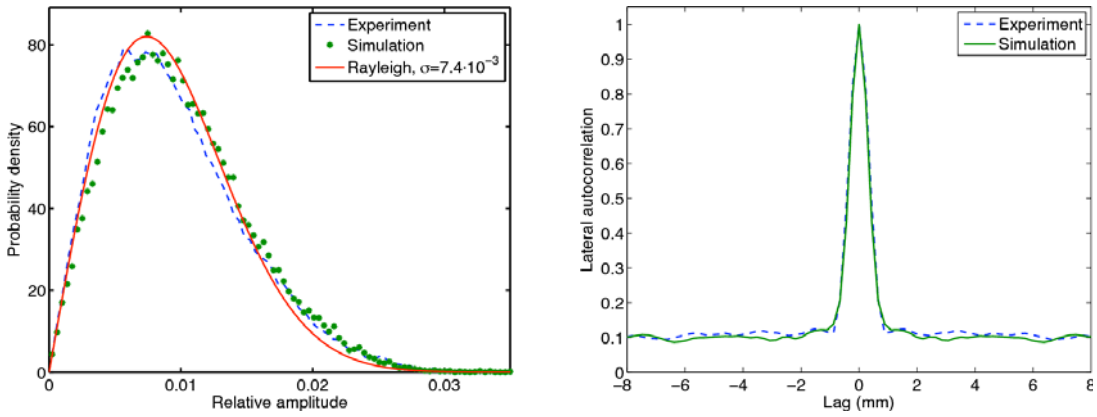

- Diffraction effects realistically modeled by convolutional approach

UNIVERSITY OF Cincinnati

For a check on the accuracy of the simulation, image statistics were compared between simulation and experiment. The plots above compare statistics for speckle amplitude within the region of interest marked by dashed lines on the previous slide.

The image amplitude follows a Rayleigh probability density function, as expected for fully-developed speckle from incoherently scattering media (Burckhardt 1978). The lateral autocorrelation function, which provides a measure of the dominant speckle length scale in the azimuthal direction, is similar between the simulation (correlation length 0.40 mm) and the measurement (correlation length 0.43 mm).

Echo decorrelation imaging

- Goal: quantitatively image severe tissue heating in thermal ablation

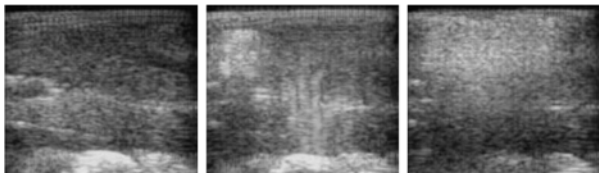

- Approach: map temporal decorrelation of complex image frames on short time scales (Δt ~ 20 ms)

Frame cross-correlation:

$$R(\mathbf{r},t) = \langle I(\mathbf{r},t)^* \, I(\mathbf{r},t+\Delta t)\rangle$$

Integrated backscatter:

$$\beta(\mathbf{r},t) = \sqrt{\langle |I(\mathbf{r},t)|^2\rangle \, \langle |I(\mathbf{r},t+\Delta t)|^2\rangle}$$

Echo decorrelation:

$$\sigma(\mathbf{r},t) = 2\,\frac{\beta(\mathbf{r},t) - R(\mathbf{r},t)}{\beta(\mathbf{r},t) + \bar{\beta}(t)}$$

UNIVERSITY OF Cincinnati

A second pulse-echo imaging method, based on the same beamformed signals usually displayed as B-scan images, is echo decorrelation imaging (Mast 2008). In this approach, a position-dependent decorrelation function is computed between adjacent pulse-echo image frames acquired at the system frame rate (about 50 Hz for the system employed here).

The echo decorrelation map $\sigma(\mathbf{r},t)$ is computed using a temporal cross-correlation between two adjacent frames as defined above, where Δt is the inverse of the system frame rate and the angular brackets represent spatial integration over a window centered at position $\mathbf{r}$. The resulting echo decorrelation is near zero for positions and times where the medium is unaffected by heating, and is substantially greater than zero where the medium is undergoing rapid changes due to thermal ablation.

Quantifying tissue changes

- Power spectra of tissue reflectivity:

$$\Gamma(\mathbf{k},t) = \int_{V_0} \gamma(\mathbf{r},t)\, e^{-i\mathbf{k}\cdot\mathbf{r}}\, dV_0$$

$$S_{mn}(\mathbf{k},\mathbf{r},t) \equiv \langle \Gamma(\mathbf{k},t+m\Delta t)^*\, \Gamma(\mathbf{k},t+n\Delta t)\rangle_{\mathbf{r}}$$

- Relations to measured backscatter:

$$\beta(\mathbf{r},t) \sim S_{00}(2k_0,\mathbf{r},t)$$

$$R(\mathbf{r},t) \sim S_{01}(2k_0,\mathbf{r},t)$$

$$\sigma(\mathbf{r},t) \approx 1 - \frac{S_{01}(2k_0,\mathbf{r},t)}{\sqrt{S_{00}(2k_0,\mathbf{r},t)\, S_{11}(2k_0,\mathbf{r},t)}}$$

- $\sigma(\boldsymbol{r},t) \approx$ decoherence of reflectivity power spectrum for lag Δt

UNIVERSITY OF Cincinnati

Echo decorrelation images can be related to intrinsic structural changes in the tissue medium using known relationships between the scattered field and tissue microstructure (Morse 1968; Waag 1993). Tissue structure is characterized by a spatial power spectrum S_{00}, defined in terms of the 3D spatial Fourier transform Γ of the medium reflectivity γ. Similarly, a cross spectrum S_{01} can be formed between the medium reflectivities at times t and $t + \Delta t$.

Under the weak scattering approximation employed here, the echo decorrelation map σ then approximates the position-dependent decoherence of the spatial power spectrum of the medium reflectivity γ. Fractional decorrelation corresponds to the fractional decoherence of this power spectrum for the temporal lag Δt. Thus, the echo decorrelation parameter can be interpreted directly as a measure of local, heat-induced changes within the scattering tissue medium.

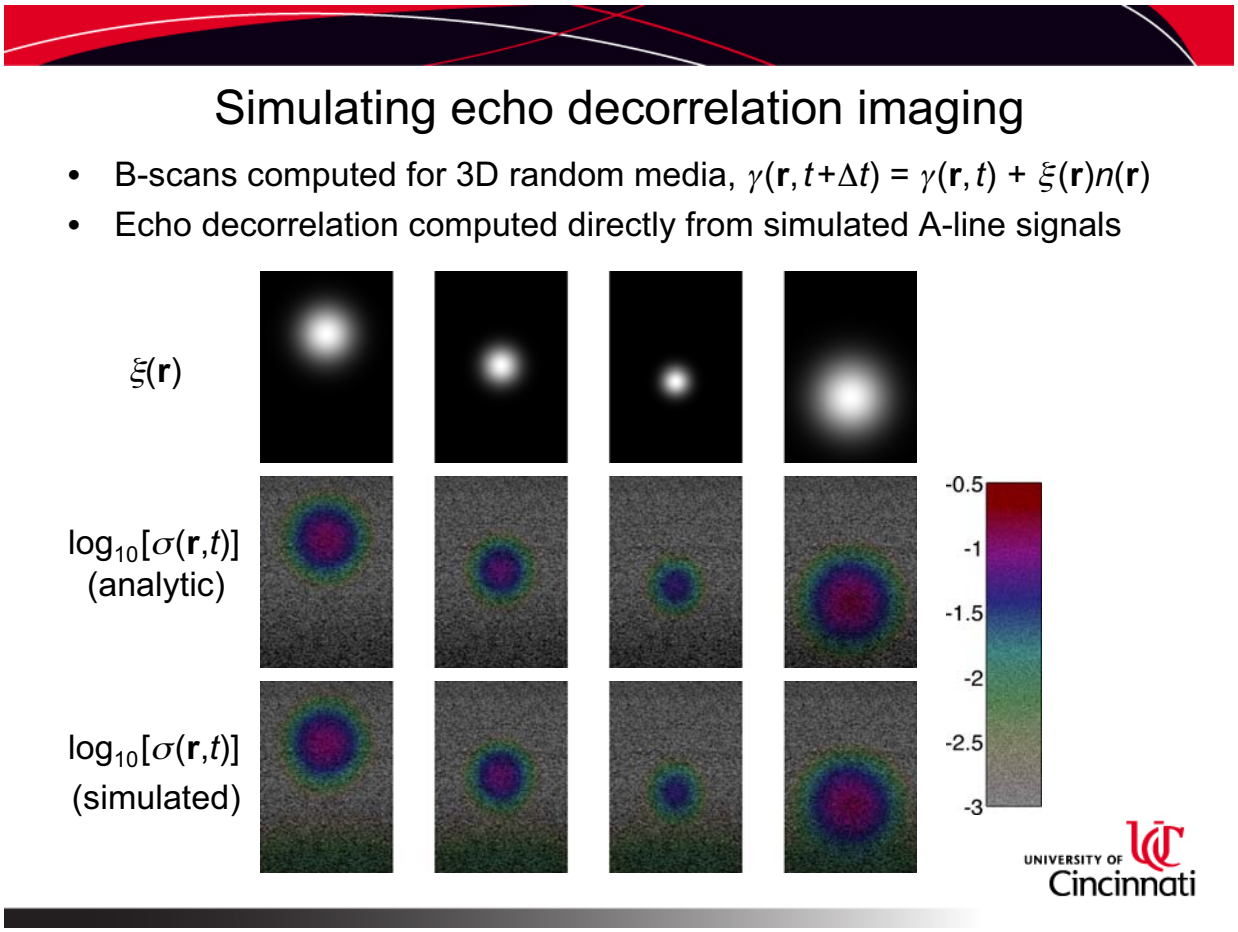

To test this interpretation of echo decorrelation imaging, simulations were performed using an imaging configuration equivalent to the B-scan simulations shown above. Spatial decoherence of a 3D random medium γ at time $t + \Delta t$ was introduced by adding Gaussian random noise $n(\mathbf{r})$, modulated by a Gaussian spatial envelope $\xi(\mathbf{r})$ (cylindrically symmetric in the out-of-plane direction).

Each column above shows simulation results for the medium variation $\xi(\mathbf{r})$ plotted on a linear scale in the first row. The second row shows the decoherence spectrum

$$\sigma(\mathbf{r}, t) \text{ (analytic)} \equiv 1 - \frac{S_{01}(2k_0, \mathbf{r}, t)}{\sqrt{S_{00}(2k_0, \mathbf{r}, t)\, S_{11}(2k_0, \mathbf{r}, t)}}$$

and the third row shows simulated echo decorrelation images. Both decoherence spectra and echo decorrelation maps are logarithmically scaled and superimposed on simulated B-scans, according to the color scale shown (Mast 2008).

These simulated echo decorrelation images agree well with the theoretical position dependent decoherence of the reflectivity power spectrum. The only substantial discrepancy seen is some decorrelation due to electronic noise at greater image depths.

In vitro radiofrequency ablation experiments

- *Ex vivo* bovine liver, radiofrequency ablation, 500 kHz, 94.8 V_{pp}
- Exposures performed until tissue impedance rise (2-13 min)
- B-scan imaging by 7 MHz linear array, 51 Hz frame rate

- Echo decorrelation imaging from A-lines sampled at 33.3 MHz

UNIVERSITY OF Cincinnati

Tests of echo decorrelation imaging were performed for radiofrequency ablation of *ex vivo* bovine liver tissue. Experimental methods were similar to a previous study (Mast 2008), except for use of a custom radiofrequency ablation needle, allowing application of a constant voltage. A total of 5 ablation exposures were performed under the above conditions. Echo decorrelation images were computed from sampled A-line data in a manner similar to the previous study (Mast 2008).

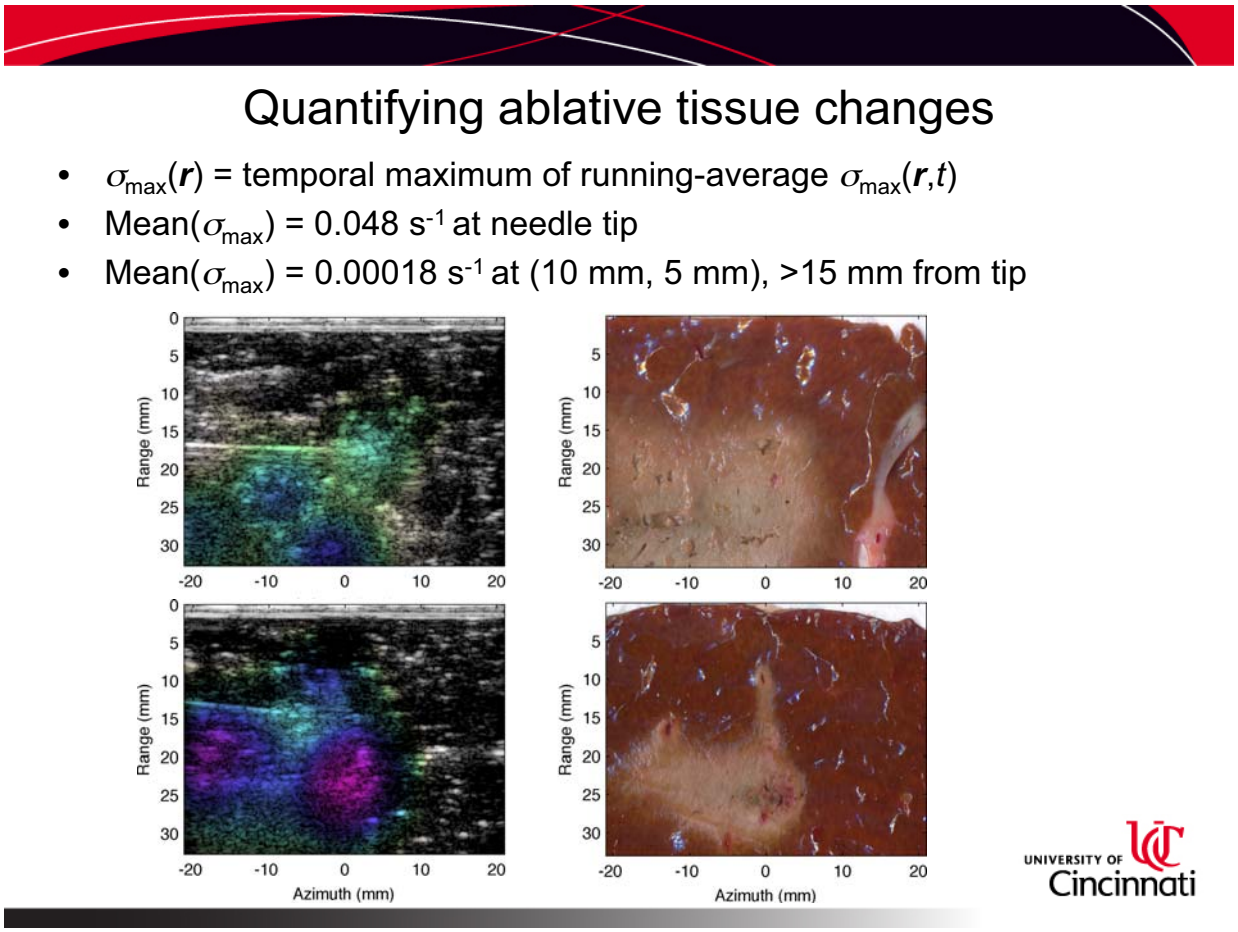

Local echo decorrelation in these experiments was computed using a temporal running average (Mast 2008). The temporal maximum of this running average is representative of the overall echo decorrelation incurred at an image location **r** during tissue ablation, and thus also representative of the overall decoherence of the medium reflectivity during the treatment.

Above, the left-column images show this position-dependent maximum echo decorrelation, logarithmically scaled and superimposed on post-treatment B-scan images computed from the same echo data. The right-column images show corresponding gross sections of treated tissue in the ultrasound image plane, registered precisely to the B-scan and echo decorrelation images. As in the previous study (Mast 2008), spatial correspondence is seen between echo decorrelation and successful tissue ablation.

Mean values of this maximum echo decorrelation across the 5 experiments was higher at the tip of the RF ablation needle ($4.8 \cdot 10^{-2} \pm 3.1 \cdot 10^{-2}$ s^{-1}) by more than two orders of magnitude than at a location outside the ablation region ($1.8 \cdot 10^{-4} \pm 1.6 \cdot 10^{-4}$ s^{-1}) . This difference is statistically significant (Student t-test, $t = 3.41$, $p = 0.027$). Thus, in these experiments, the temporal decoherence of the medium reflectivity was significantly greater for tissue undergoing thermal ablation.

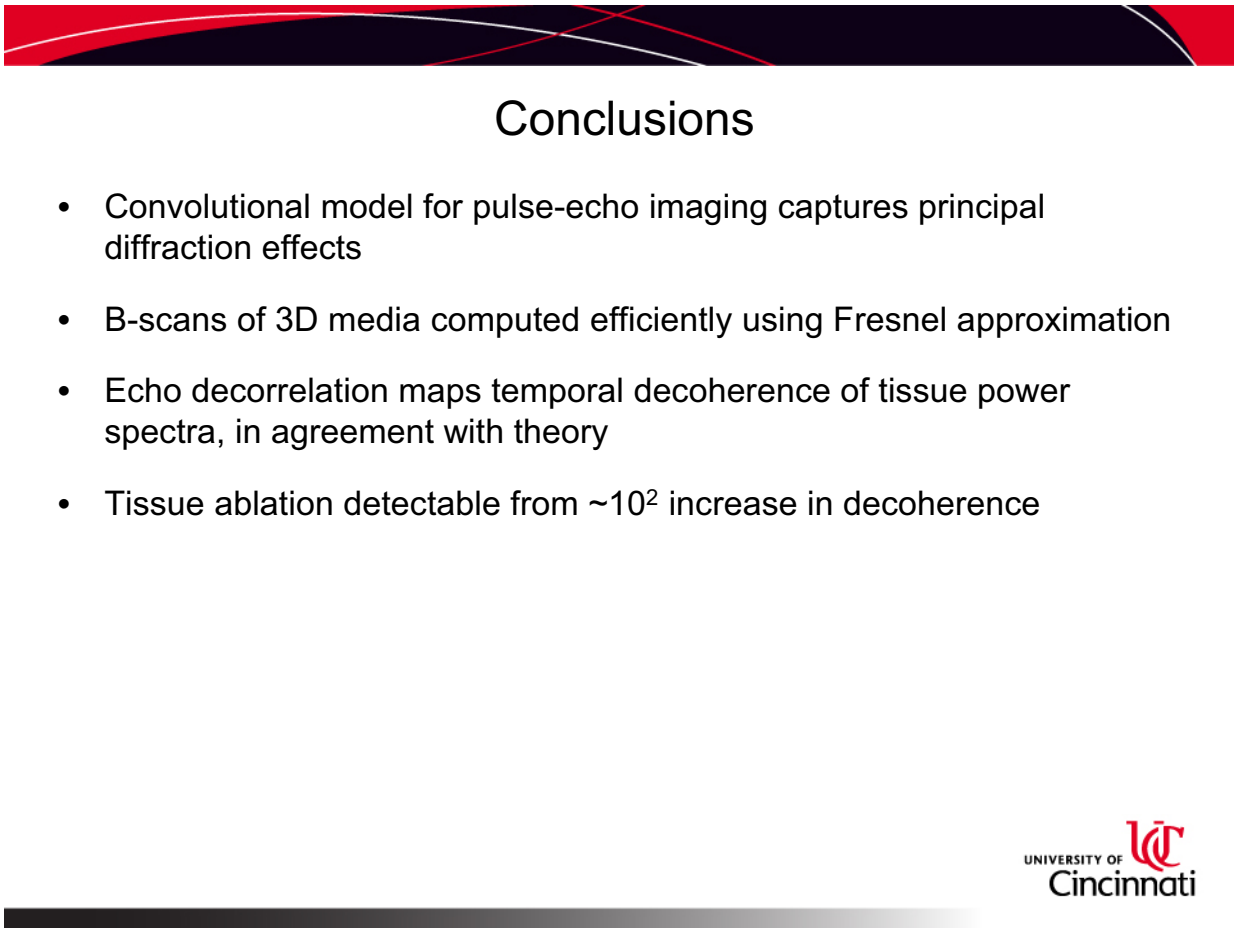

In conclusion, the analytic and numerical methods presented here are capable of modeling pulse-echo imaging, including B-scan and echo decorrelation imaging. With small modifications, the same methods can be applied to other ultrasound imaging methods such as passive cavitation imaging (Salgaonkar 2009). In either case, computation of the system function Λ by numerical methods such as the Fresnel approximation (Mast 2007) is useful for efficient computations. Alternate efficient approaches to computing the system function, such as fast-nearfield and angular-spectrum methods (Zeng 2009), are also feasible.

Applied to echo decorrelation imaging, this analytic approach has demonstrated the approximate equivalence between local echo decorrelation and local decoherence of the spatial power spectrum for the medium reflectivity. A large increase in echo decorrelation (or equivalently, decoherence of tissue reflectivity) is useful for detecting local tissue ablation, with potential applications to guidance and control of radiofrequency ablation and other thermal therapies for cancer treatment.

Acknowledgments

- Biomedical Acoustics Laboratory: Amel Alqadah, William Bowlus, Mark Burgess, Kevin Haworth, Chandra Priya Karunakaran, Anna Nagle, Dan Pucke, Jason Raymond, Kyle Rich, Vasant Salgaonkar
- Clinical collaborators: Joseph Buell, Steven Rudich
- NIH: grants R43 CA124283 and R21 EB008483

References

Burckhardt CB. Speckle in ultrasound B-mode scans. IEEE Trans Son Ultrason **25**, 1–6 (1978).

Jansson TT, Mast TD, Waag RC. Measurements of differential scattering cross-section using a ring transducer. J Acoust Soc Am **103**, 3169–3179 (1998).

Mast TD. Fresnel approximations for ultrasonic fields of rectangularly symmetric sources. J Acoust Soc Am **121**, 3311–3322 (2007).

Mast TD, Pucke DP, Subramanian SE, Bowlus WJ, Rudich SM, Buell JF. Ultrasonic monitoring of in vitro radiofrequency ablation by echo decorrelation imaging. J Ultrasound Med **27**, 1685–1697 (2008).

Mast TD. Convolutional modeling of diffraction effects in pulse-echo ultrasound imaging. J Acoust Soc Am, in press (2010).

Morse PM, Ingard KU. *Theoretical Acoustics* (McGraw-Hill, New York NY, 1968), Ch. 8.

Salgaonkar VA, Datta S, Holland CK, Mast TD. Passive cavitation imaging with ultrasound arrays. J Acoust Soc Am **126**, 3071–3083 (2009).

Waag RC, Astheimer JP. Measurement system effects in ultrasound scattering experiments. In *Ultrasonic Scattering in Biological Tissues* (Shung KK, Thieme GA, eds.; CRC, Boca Raton FL, 1993), Ch. 8.

Zeng X, McGough RJ. Optimal simulations of ultrasonic fields produced by large thermal therapy arrays using the angular spectrum approach. J Acoust Soc Am **125**, 2967–2977 (2009).